ADVANCED ELECTROMAGNETICS, VOL. 8, NO. 3, MAY 2019

Study of Stacked High T_c Superconducting Circular Disk Microstrip Antenna in Multilayered Substrate Containing Isotropic and/or Uniaxial Anisotropic Materials

Akrame Sofiane Boughrara[1], Siham Benkouda[2], Abdelouahab Bouraiou[1], and Tarek Fortaki[1]*

[1]Electronics Department, University of Batna 2, Batna, Algeria
[2] Electronics Department, University of Constantine 1, Constantine, Algeria
*corresponding author, E-mail: t_fortaki@yahoo.fr

Abstract

In this paper, we present a rigorous full-wave analysis able to estimate exactly the resonant characteristics of stacked high T_c superconducting circular disk microstrip antenna. The superconducting patches are assumed to be embedded in a multilayered substrate containing isotropic and/or uniaxial anisotropic materials (the analysis is valid for an arbitrary number of layers). London's equations and the two-fluid model of Gorter and Casimir are used in the calculation of the complex surface impedance of the superconducting circular disks. Numerical results are presented for a single layer structure as well as for two stacked circular disks fabricated on a double-layered substrate.

1. Introduction

The need for high data transmission rate coupled with ever increasing demand for mobile devices has generated a great interest in low cost, compact microwave and millimeter-wave antennas exhibiting high gain and wide bandwidth. Owing to their many attractive features and excellent advantages [1], microstrip antennas have attracted attention in both theoretical research and engineering applications over the past decades. Microstrip antennas are used in an increasing number of applications, ranging from biomedical diagnosis to wireless communication [2], [3]. However, as typical disadvantages are their capability to resonate at a single frequency, narrow bandwidth and low gain [4].

The discovery of high T_c superconductor oxides has made possible a new class of microwave and millimeter-wave devices operating at temperatures considerably above liquid helium temperatures. Passive microwave components are among the first practical devices fabricated from these high T_c materials in which the surface resistance is a measure of the device performance at any frequency [5]. The extremely low surface resistance of superconductors facilitates the development of microwave devices with better performance than conventional devices [6]. The low surface resistance corresponds to a large quality factor and improved performance such as higher gain and lower insertion loss in passive microwave devices [7]. However, the narrow bandwidth that occurs with large quality factor is a major obstacle to the wider application of superconducting microstrip antennas [6], [7].

While maintaining the advantages of conventional single patch microstrip antennas, microstrip antennas of stacked configuration, consisting of one or more patches parasitically coupled to a driven patch, overcome the inherent narrow bandwidth limitation by introducing additional resonances in the frequency range of operation, achieving wide bandwidths [8], [9]. In addition, stacked microstrip configurations offer the possibility of dual-frequency operation [8], [10].

In this paper, we present a rigorous full-wave analysis of stacked high Tc superconducting circular disk microstrip antenna. We consider that the radiating elements are embedded in a multilayered structure containing isotropic and/or uniaxial anisotropic materials. Although the theoretical analysis presented in the current paper is valid for an arbitrary number of layers, we give here only numerical results for a single layer structure as well as for two-stacked circular disks fabricated on a double-layer substrate. The paper is organized as follows. In section 2, we develop new explicit expressions for the evaluation of the spectral dyadic Green's functions of two stacked circular disks embedded in a multilayered medium. These new expressions are also valid for structures involving more than two circular disks. London's equations and the two-fluid model of Gorter and Casimir are used in the calculation of the complex surface impedance of the superconducting circular disks. In section 3, to validate the proposed approach, our numerical results are compared with theoretical and experimental data available in the literature for two different configurations. The first configuration consists on a single superconducting patch on a grounded dielectric substrate, while, the second configuration is composed of two stacked circular disks fabricated on a double-layer substrate. Finally concluding remarks are summarized in section 4.

2. Formulation

Figure 1 shows the geometry of two stacked high T_c superconducting circular microstrip patches fabricated with

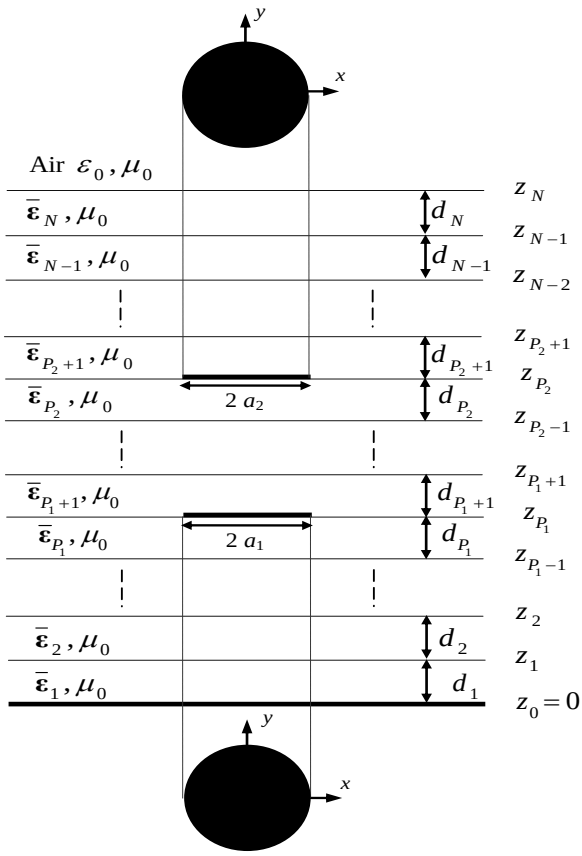

Figure 1: Two high T_c superconducting circular disk microstrip antenna in a stacked configuration.

the same superconducting material. The radii of the bottom patch of thickness e_1 and the top one of thickness e_2 are, respectively, a_1 and a_2. The multilayered medium is constituted of N uniaxial anisotropic layers with the optical axis normal to the patches. Each layer of thickness $d_j = z_j - z_{j-1}$ is characterized by the free-space permeability μ_0 and a permittivity tensor of the form

$$\bar{\varepsilon}_j = \varepsilon_0 \,\mathrm{diag}\left[\varepsilon_{xj}, \varepsilon_{xj}, \varepsilon_{zj}\right] \qquad (1)$$

In equation (1), ε_0 is the free-space permittivity and diag stands for the diagonal matrix with the diagonal elements appearing between the brackets. Equation (1) can be specialized to the isotropic substrate by allowing $\varepsilon_{xj} = \varepsilon_{zj} = \varepsilon_{rj}$. The patches are embedded in the stratification at the interface planes $z = z_{P_1}$ and $z = z_{P_2}$. All fields and currents are time harmonic with the $e^{i\omega t}$ time dependence suppressed. Let $\mathbf{J}^i(\rho,\phi) = \left[\; J^i_\rho(\rho,\phi) \quad J^i_\phi(\rho,\phi)\right]^T$ (*where T implies transpose and* $i = 1, 2$) be the surface current density on the disc of radius a_i. Also, let $\mathbf{E}^i(\rho,\phi,z_{P_i}) = \left[\; E^i_\rho(\rho,\phi,z_{P_i}) \quad E^i_\phi(\rho,\phi,z_{P_i})\right]^T$ be the value of the transverse electric field at the plane of the patch of radius a_i. Owing to the revolution symmetry of the multilayered medium of figure 1 around the z-axis, when the Helmholtz equations for the longitudinal field components E_z and H_z are solved in cylindrical coordinates inside each of the layers of that medium, it turns out that the dependence of E_z and H_z on the ϕ coordinate is of type $e^{ik\phi}$ (*where k is an integer*), as a consequence, $\mathbf{J}^i(\rho,\phi)$ and $\mathbf{E}^i(\rho,\phi,z_{P_i})$ can be written as

$$\mathbf{J}^i(\rho,\phi) = \sum_{k=-\infty}^{+\infty} e^{ik\phi}\mathbf{J}^i_k(\rho) \qquad (2)$$

$$\mathbf{E}^i(\rho,\phi,z_{P_i}) = \sum_{k=-\infty}^{+\infty} e^{ik\phi}\mathbf{E}^i_k(\rho,z_{P_i}) \qquad (3)$$

Following a mathematical reasoning similar to that shown in [1], we obtain a relation among $\mathbf{J}^1(\rho,\phi)$, $\mathbf{J}^2(\rho,\phi)$, $\mathbf{E}^1(\rho,\phi,z_{P_1})$, and $\mathbf{E}^2(\rho,\phi,z_{P_2})$ in the spectral domain given by

$$\mathbf{e}^1_k(k_\rho, z_{P_1}) = \bar{\mathbf{G}}^{11}(k_\rho).\mathbf{j}^1_k(k_\rho) + \bar{\mathbf{G}}^{12}(k_\rho).\mathbf{j}^2_k(k_\rho) \qquad (4)$$

$$\mathbf{e}^2_k(k_\rho, z_{P_2}) = \bar{\mathbf{G}}^{21}(k_\rho).\mathbf{j}^1_k(k_\rho) + \bar{\mathbf{G}}^{22}(k_\rho).\mathbf{j}^2_k(k_\rho) \qquad (5)$$

where $\mathbf{j}^i_k(k_\rho)$ and $\mathbf{e}^i_k(k_\rho, z_{P_i})$ are, respectively, the vector Hankel transforms of $\mathbf{J}^i_k(\rho)$ and $\mathbf{E}^i_k(\rho, z_{P_i})$, and the *nm* element of the dyadic Green's functions is given by

$$\bar{\mathbf{G}}^{nm}(k_\rho) = \bar{\mathbf{\Gamma}}^{12}_{<n}.\left[\bar{\mathbf{g}}_0.\bar{\mathbf{\Gamma}}^{12}_{>m} - \bar{\mathbf{\Gamma}}^{22}_{>m}\right].\left[\bar{\mathbf{g}}_0.\bar{\mathbf{\Gamma}}^{12}_{=} - \bar{\mathbf{\Gamma}}^{22}_{=}\right]^{-1} = \bar{\mathbf{G}}^{mn}(k_\rho) \qquad (6)$$

with

$$\bar{\mathbf{\Gamma}}_{<n} = \prod_{j=P_n}^{1}\bar{\mathbf{T}}_j\,.\,\bar{\mathbf{\Gamma}}_{>m} = \prod_{j=N}^{P_m+1}\bar{\mathbf{T}}_j\,.\,\bar{\mathbf{\Gamma}}_{=} = \prod_{j=N}^{1}\bar{\mathbf{T}}_j \qquad (7)$$

In (7), $\bar{\mathbf{T}}_j$ is the matrix representation of the j^{th} layer in the (TM, TE) representation [2]. It is to be noted that $\bar{\mathbf{G}}^{11}$ is related to the bottom disk and $\bar{\mathbf{G}}^{22}$ is related to the top disk. The dyadic Green's functions $\bar{\mathbf{G}}^{12}$ and $\bar{\mathbf{G}}^{21}$ characterize the coupling between the bottom patch and the top patch. Whatever the number of layers in the stacked configuration, the new explicit expression shown in equation (6) allows the computation of the dyadic Green's functions easily using simple matrix multiplications. Note also that the expression given in (6) is valid for stacked configurations containing more than two circular disks.

Unlike the case of perfectly conducting patches, the transverse electric field does not vanish on the area of high Tc superconducting patches. This is because the superconductor shows a resistance, although the value of this resistance is very small. The two-fluid model can be used to explain the general behavior of superconductors at microwave frequencies. The two-fluid model treats the current carriers in the superconductors as being of two

distinct types: a supercarrier fraction, which carries current without any dissipation, and a normal fraction, which exhibit resistive scattering similar to the electrons in normal metals.

Considering the superconducting effects, we need simply to modify equations (4) and (5) by replacing $\overline{\mathbf{G}}^{11}(k_\rho)$ by $\overline{\mathbf{G}}_s^{11}(k_\rho) = \overline{\mathbf{G}}^{11}(k_\rho) - Z_{s1}\cdot\overline{\mathbf{I}}$ and $\overline{\mathbf{G}}^{22}(k_\rho)$ by $\overline{\mathbf{G}}_s^{22}(k_\rho) = \overline{\mathbf{G}}^{22}(k_\rho) - Z_{s2}\cdot\overline{\mathbf{I}}$, where Z_{s1} and Z_{s2} are, respectively, the surface impedance of the bottom and top superconducting patches and $\overline{\mathbf{I}}$ stands for the 2x2 unit matrix. When the thicknesses of the superconducting circular disks are less than three times the zero-temperature penetration depth (λ_0), Z_{s1} and Z_{s2} can be expressed as follows [7]:

$$Z_{s1} = \frac{1}{\sigma e_1},\ Z_{s2} = \frac{1}{\sigma e_2} \tag{8}$$

where σ is the complex conductivity of the superconducting films. It is determined by using London's equation and the Gorter-Casimir two-fluid model as [7]

$$\sigma = \sigma_1 - i\sigma_2 \tag{9}$$

The resistive part of the complex conductivity (σ_1) may arise from normal electron conduction within non-superconducting grains and scattering from grain boundaries, flux vibration at pinning centers, and normal electron conduction due to thermal agitation in the superconducting state. The temperature dependence of σ_1 is as follows [7]:

$$\sigma_1 = \sigma_n\left(\frac{T}{T_c}\right)^4 \tag{10}$$

where T is the temperature, T_c is the transition temperature of the superconductor and σ_n is the normal state conductivity at $T = T_c$. The reactive part of the conductivity $(-i\sigma_2)$ arises from the lossless motion of the superconducting carriers which may be derived directly from the Lorentz-force equation as [5]:

$$\sigma_2 = \frac{1}{\omega\mu_0[\lambda(T)]^2} \tag{11}$$

with

$$\lambda(T) = \frac{\lambda_0}{\sqrt{1-\left(\frac{T}{T_c}\right)^4}} \tag{12}$$

In equation (11), ω is the angular frequency and $\lambda(T)$ is the London penetration depth at temperature T. Now, that we have include the effect of the superconductivity of circular disks in the Green's functions formulation, the Galerkin procedure of the moment method can be easily applied to obtain the complex resonant frequencies of the stacked high Tc superconducting circular disk microstrip antenna.

Table 1: Comparison of our calculated resonant frequencies with those obtained via the modified cavity model of Richard *et al.* [11].

a (mm)	Resonant Frequencies (GHz)		Error (%)
	Our results	Cavity model [11]	
5.3	3.400	3.317	2.44
5.6	3.218	3.144	2.30
5.9	3.055	2.987	2.23
6.2	2.907	2.845	2.13
6.6	2.731	2.676	2.01
7.0	2.575	2.526	1.90

3. Validation of the proposed approach

For a circular radiating element the resonant modes are denoted by TM_{nm}, where *n* and *m* denote variations in the azimuthal and radial directions, respectively. In the following only results for the TM_{11} mode are presented. This fundamental mode is characterized by the resonant frequency f_r^{11}, which is the lowest resonant frequency. Note that the proposed approach can give results not only for the fundamental mode but also for high order modes. If we want to calculate the resonant frequency for a specific mode, it is important to choose the basis functions such that they include qualitative natures of the true unknown current distributions of this mode. Also, the values of the three initial guesses used in the Muller's method for root seeking of the characteristic equation should be taken close to the resonant frequency of the considered mode. To this end, we can use the magnetic wall cavity model to obtain the values of the three guesses. In order to validate the proposed method for the case of a single circular disc printed on a one-layered substrate, we compare in Table 1 our numerical results with those obtained via the modified magnetic wall cavity model [11].

The circular disc is fabricated using a YBCO (YBa2Cu3O7) superconducting thin film of thickness $e = 350\text{nm}$ with a normal state conductivity at the transition temperature $\sigma_n = 10^6\,\text{S/M}$, a zero-temperature penetration depth $\lambda_0 = 140\text{nm}$ and a transition temperature $T_c = 89\,\text{K}$. The circular disc is printed on a lanthanum aluminate substrate (LaAIO3) of thickness $d = 254\mu\text{m}$ and permittivity $\varepsilon_r = 23.81$. The lanthanum aluminate substrate was chosen in the experiment of Richard et al. [11] despite its high permittivity because it allows the growth of high-quality (low surface resistance) YBCO superconducting films [11]. The operating temperature is $T = 77\,\text{K}$. Table 1 summarizes

Table 2: Comparison of calculated lower and upper resonant frequencies with experimental data, for two stacked circular disks fabricated on a two-layered Substrate; $\varepsilon_{r1} = \varepsilon_{r2} = 2.47$, $d_1 = d_2 = 750\,\mu\text{m}$, $a = 0.5\,\text{cm}$, $\varepsilon_r = 2.32$. $a_1 = 18.9\,\text{mm}$.

Top disk radius a_2 (mm)	Lower resonant f_l^{11}, Upper resonant f_u^{11}			
	Measured Long and Walton [12]		Our results	
	f_l^{11} (GHz)	f_u^{11} (GHz)	f_l^{11} (GHz)	f_u^{11} (GHz)
17.5	2.853	3.338	2.854	3.341
18.75	2.830	3.120	2.829	3.117
18.9	2.825	3.110	2.818	3.107
19.25	2.804	3.060	2.805	3.069
20	2.728	3.009	2.731	3.006

the calculated resonant frequencies and those obtained via the modified cavity model [11] for different radii of the superconducting circular disk and differences between these two results less than 2.5% are obtained. Note that the small differences between our numerical results and those obtained via the modified cavity model can be attributed to the fact that the cavity model do not account rigorously for the effect of fringing fields, especially for thick substrates.

A standard configuration for a microstrip antenna is a single patch supported above a ground plane by a simple dielectric substrate. This is a simple configuration that is relatively easy to fabricate, but it is limited in its functional capabilities. Dual-frequency structures are useful in situations where the antenna is required to operate efficiently at two distinct frequencies. Conventional microstrip antennas do not guarantee this type of operation. A more complex configuration, consisting of two microstrip patches in a stacked configuration, offers performance features that are not usually obtainable from the single-patch single-dielectric configuration. These features include wider bandwidth and dual-frequency characteristics. In order to validate the proposed theory for the case of two stacked circular disks, numerical results are obtained for the parameters used in the experiment of Long and Walton [12]. The dielectric substrate is made of two layers of the same material and identical thickness. $\left(\varepsilon_{r1} = \varepsilon_{r2} = 2.47 \text{ et } d_1 = d_2 = 750\,\mu\text{m}\right)$. The radius of the bottom metallic disc is $a_1 = 18.9\,\text{mm}$ whereas that of the top metallic disc is considered variable. Due to the presence of the top patch in the stacked configuration, two resonances associated with the two constitutive resonators of the stacked structure are obtained. The lower resonance is noted f_l^{11} while the upper resonance is noted f_u^{11}. In Table 2, we have given at the same time the lower resonance and the upper resonance. It is observed from these comparisons that the agreement between theory and experiment is excellent.

In section 2, we have shown that the new explicit expression for the evaluation of the dyadic Green's functions is valid for stacked configurations containing more than two circular disks. Hence, the proposed method can be easily applied to compute the complex resonant frequencies of stacked microstrip antennas with three radiating elements.

4. Conclusions

A rigorous full-wave analysis able to estimate exactly the resonant characteristics of stacked high T_c superconducting circular disk microstrip antenna has been presented. The superconducting circular disks are embedded in a multilayered structure containing isotropic and/or uniaxial anisotropic materials. London's equations and the two-fluid model of Gorter and Casimir have been used in the calculation of the complex surface impedance of the superconducting circular disks. New explicit expressions for the evaluation of the dyadic Green's functions of two stacked circular disks fabricated on a multilayered substrate have been derived. These expressions are also valid for stacked configurations containing more than two patches. Contrary to the equivalent boundary method [13], no transformation is required when the developed Green's functions are used in the moment method analysis of stacked high T_c superconducting rectangular microstrip patches. The numerical results obtained are compared with previously published numerical results and with measurements. Good agreement is found in all cases among all sets of results.

References

[1] S. Bedra, R. Bedra, S. Benkouda, T. Fortaki, Efficient full-wave analysis of inverted circular microstrip antenna, Microwave and Optical Technology Letters, 56: 2422-2425, 2014.

[2] M. Amir, S. Bedra, S. Benkouda, T. Fortaki, Bacterial foraging optimisation and method of moments for modelling and optimisation of microstrip antennas, IET Microwaves, Antennas & Propagation, 8: 295-300, 2014.

[3] S. Bedra, S. Benkouda, T. Fortaki, Analysis of a circular microstrip antenna on isotropic or uniaxially anisotropic substrate using neurospectral approach, COMPEL: The International Journal for Computation and Mathematics in Electrical and Electronic Engineering, 33: 567-580, 2014.

[4] S. Shekhawat, P. Sekra, D. Bhatnagar, V. K. Saxena, J.S. Saini, Stacked arrangement of rectangular microstrip patches for circularly polarized broadband

performance, IEEE Antennas and Wireless Propagation Letters, 9: 910-913, 2010.

[5] F. Chebbara, S. Benkouda, T. Fortaki, Fourier transform domain analysis of high Tc superconducting rectangular microstrip patch over ground plane with rectangular aperture, Journal of Infrared, Millimeter, and Terahertz Waves, 31: 821-832, 2010.

[6] S. Benkouda, M. Amir, T. Fortaki, A. Benghalia, Dual-frequency behaviour of stacked high Tc superconducting microstrip patches, Journal of Infrared, Millimeter, and Terahertz Waves, 32: 1350-1366, 2011.

[7] S. Benkouda, A. Messai, M. Amir, S. Bedra, T. Fortaki, Characteristics of a high Tc superconducting rectangular microstrip patch on uniaxially anisotropic substrate, Physica C Superconductivity and its Applications, 502: 70-75, 2014.

[8] T. Fortaki, L. Djouane, F. Chebbara, A. Benghalia, On the dual-frequency behavior of stacked microstrip patches, IEEE Antennas and Wireless Propagation Letters, 7: 310-313, 2008.

[9] A.S. Elkorany, S.M Elhalafawy, A. Radwan, G.G. Gentili, Design of stacked segmented ultra wide band antenna, Proc. LAPC16, Loughborough, United Kingdom, pp. 1−4, 2016.

[10] Z. Liang, J. Liu, Y. Li, Y. Long, A Dual-frequency broadband design of coupled-fed stacked microstrip monopolar patch antenna for WLAN applications, IEEE Antennas and Wireless Propagation Letters, 15: 1289-1292, 2016.

[11] M.A. Richard, K.B. Bhasin, P.C. Claspy, Superconducting microstrip antennas: an experimental comparison of two feeding, IEEE Transactions on Antennas and Propagation, 41: 967-974, 1993.

[12] S.A. Long, M.D. Walton, A dual-frequency stacked circular-disk antenna, IEEE Transactions on Antennas and Propagation, AP-27: 270-273, 1979.

[13] T. Fortaki, L. Djouane, F. Chebbara, A. Benghalia, Radiation of rectangular microstrip patch antenna covered with a dielectric layer, International Journal of Electronics, 95: 989-998, 2008.